# Block model versus thermomechanical model: new insights on the present-day regional deformation in the surroundings of the Calabrian Arc

Raffaele Splendore, Anna Maria Marotta, Riccardo Barzaghi, Alessandra Borghi and Letizia Cannizzaro

*Geological Society, London, Special Publications* 2010; v. 332; p. 129-147
doi:10.1144/SP332.9

# Block model versus thermomechanical model: new insights on the present-day regional deformation in the surroundings of the Calabrian Arc

RAFFAELE SPLENDORE[1]*, ANNA MARIA MAROTTA[1], RICCARDO BARZAGHI[2], ALESSANDRA BORGHI[3] & LETIZIA CANNIZZARO[2]

[1]*Università degli Studi di Milano, Department of Earth Sciences 'Ardito Desio', Section of Geophysics, L. Cicognara 7, 20129 Milan, Italy*

[2]*DIIAR, Department of Environmental, Hydraulic, Infrastructures and Surveying, Engineering Politecnico di Milano, Piazza Leonardo da Vinci 32, 20133 Milano, Italy*

[3]*OGS-Trieste, c/o DIIAR, Department of Environmental, Hydraulic, Infrastructures and Surveying, Engineering Politecnico di Milano, Piazza Leonardo da Vinci 32, 20133 Milano, Italy*

**Corresponding author (e-mail: raffaele.splendore@unimi.it)*

**Abstract:** A finite-element thermomechanical model is used to analyse present-day crustal deformation in the surroundings of the Calabrian Arc. The major structural complexities of the Tyrrhenian area are taken into account, along with the rheological properties of the rocks resulting from a thermal analysis. A comparison between the results obtained from a model composed of three wide rheologically uniform blocks and those obtained from the thermomechanical model allows us to better constrain the geophysical assumptions and shed light on the roles of the different active mechanisms acting in the Tyrrhenian. Our comparative analysis enlightens the crucial role played by lateral rheological heterogeneities when deformation is analysed at short wavelengths of a few hundred kilometres of the Tyrrhenian, driving the observed diffuse SW–NE extension within the regional context of active Africa–Eurasia convergence. Furthermore, a $\chi^2$ analysis based on comparisons with GPS data confirms the hypothesis that a significant part of the Africa–Eurasia convergence is absorbed through the Calabrian subduction.

Present-day crustal deformation in the Tyrrhenian is the result of a complex interplay of various dynamic processes acting at both local (e.g. faults processes) and regional scales (e.g. Africa–Eurasia convergence and Calabrian subduction). A great variability in thermal regime, surface heat flow (Pollack *et al.* 1993; Artemieva & Mooney 2001; Artemieva 2006) and crustal thickness (Bassin *et al.* 2000; Tesauro *et al.* 2008) also characterizes the central Mediterranean and the Italian Peninsula, inducing horizontal heterogeneities in the rheology through the Tyrrhenian area. The combination of the different tectonic mechanisms and the rheological heterogeneities generates an enigmatic regional deformation pattern in which areas subjected to extension, such as the Tyrrhenian and Provencal basins, are embedded in areas subjected to compression and strong crustal thickening, such as the Alps and the Appennine.

New advanced GPS (Global Positioning System) techniques and long geodetic time series make it possible to monitor this deformation with more accuracy at different length and timescales. In addition, geodetic data better constrain the geophysical forward modelling (e.g. Jiménez-Munt *et al.* 2003; Marotta *et al.* 2004; Negredo *et al.* 2004; Wang & Zheng-Ren 2006) used to test different geodynamic hypotheses in the area that were originally constrained using the geological global models NUVEL-1 or NUVEL-1A (DeMets *et al.* 1994; DeMets & Dixon 1999). The inadequacy of global models NUVEL-1 and NUVEL-1A in reproducing present-day relative plate motion has been widely demonstrated by several recent geodetic and numerical studies (among others, Sella *et al.* 2002; Fernandes *et al.* 2003; Nocquet & Calais 2003; Kremer *et al.* 2003; Marotta & Sabadini 2008). In Marotta & Sabadini's (2008) comparative analysis, the authors show that the geodetically constrained tectonic models in the Tyrrhenian area predict a regional deformation that is in better agreement with the observed deformation compared to models constrained with geological data. However, one major limitation of Marotta and

*From*: SPALLA, M. I., MAROTTA, A. M. & GOSSO, G. (eds) *Advances in Interpretation of Geological Processes: Refinement of Multi-scale Data and Integration in Numerical Modelling*. Geological Society, London, Special Publications, **332**, 129–147. DOI: 10.1144/SP332.9 0305-8719/10/$15.00 

Sabadini's model is the lack of an appropriate coupling between the rheological properties of the lithosphere and the regional thermal field.

One main advancement characterizes the present tectonic analysis with respect to Marotta & Sabadini (2008). This approach accounts for three wide rheological uniform units: the stiff East Europe platform (light grey in Fig. 1a); the European plate (intermediate grey in Fig. 1a); and the soft Mediterranean domain (dark grey in Fig. 1a). Marotta *et al.* (2004) show that a rheological averaged block model can reproduce the observed deformation at the long wavelengths ranging from several hundred to thousands of kilometres. However, when deformation is analysed at the shorter wavelengths of a few hundred kilometres, a deeper knowledge of lithosphere rheology is needed. Within a more localized analysis focused on the Tyrrhenian, Marotta & Sabadini (2008) showed, for example, that a further rheological differentiation between the Tyrrhenian and the Adria microplate (either as an unique block or subdivided into two blocks) is needed to predict at least part of the extensional component of the strain-rate tensor observed within the Tyrrhenian.

To improve this analysis a detailed thermal analysis is performed in the present study with the aim of evaluating a rheological structure of the lithosphere, relative to the Mediterranean, that is more realistic than that in Marotta & Sabadini (2008). The results of the present analysis will be discussed in comparison to the models of Marotta *et al.* (2004) and Marotta & Sabadini (2008), referred to as the 'block model' for the remainder of this paper.

## Numerical model

### *Tectonic analysis*

Tectonic deformation in the central Mediterranean is obtained using a finite-element model based on the spherical thin-sheet approach developed by Marotta *et al.* (2004). The vertically integrated momentum equations

$$\frac{\partial}{\partial\theta}\left[2\bar{\mu}\left(\frac{\partial}{\partial\theta}u_\theta+u_\mathrm{r}\right)\right]+\frac{1}{\sin\theta}\frac{\partial}{\partial\phi}\left[\bar{\mu}\left(\frac{1}{\sin\theta}\frac{\partial}{\partial\phi}u_\theta+\frac{\partial}{\partial\theta}u_\phi-u_\phi\cot\theta\right)\right]+\left[2\bar{\mu}\left(\frac{\partial}{\partial\theta}u_\theta-\frac{1}{\sin\theta}\frac{\partial}{\partial\phi}u_\phi-u_\theta\cot\theta\right)\right]\cot\theta=\frac{g\rho_\mathrm{c}R}{2L}\left(1-\frac{\rho_\mathrm{c}}{\rho_\mathrm{m}}\right)\frac{\partial}{\partial\theta}S^2 \quad (1)$$

$$\frac{\partial}{\partial\theta}\left[\bar{\mu}\left(\frac{1}{\sin\theta}\frac{\partial}{\partial\Phi}u_\theta+\frac{\partial}{\partial\theta}u_\Phi-u_\Phi\cot\theta\right)\right]+\frac{1}{\sin\theta}\frac{\partial}{\partial\Phi}\left[2\bar{\mu}\left(\frac{1}{\sin\theta}\frac{\partial}{\partial\Phi}u_\theta+\frac{\partial}{\partial\theta}u_\Phi-u_\Phi\cot\theta\right)\right]\times\cot\theta=\frac{g\rho_\mathrm{c}\mathrm{R}}{2L}\left(1-\frac{\rho_\mathrm{c}}{\rho_\mathrm{m}}\right)\frac{1}{\sin\theta}\frac{\partial}{\partial\Phi}S^2 \quad (2)$$

are solved within a 2D grid composed of linear triangular elements extending through Western Europe (Fig. 1a). $u_\theta$, $u_\phi$ and $u_\mathrm{r}$ are the velocity components along the colatitudes, longitude and the radius, $\theta$ is the colatitude, $\phi$ is the longitude, $\bar{\mu}$ the effective viscosity of the lithosphere, $S$ is the crustal thickness, $L$ is the lithosphere thickness, $\rho_\mathrm{c}$ and $\rho_\mathrm{m}$ are the density of the crust and the mantle, $g$ is the acceleration of gravity and $R$ is the terrestrial radius. The crustal thickness variation used in the present analysis is obtained from a linear interpolation onto the adopted grid of model CRUST 2.0 (Bassin *et al.* 2000).

Boundary conditions are expressed in terms of velocities. With the exception of the southern boundary of the model, boundary conditions are the same as for the best-fit model of Marotta *et al.* (2004): (1) at the western boundary of the model, located along the Mid-Atlantic Ridge, zero velocities are assumed (dashed thick line in Fig. 1a), in agreement with the concept that the effects of ridge push forces are negligible at the long wavelengths representative of Europe; (2) along the Aegean trench, trench suction forces (white arrows in Fig. 1a) are based on the geodetic velocities determined by McClusky *et al.* (2000) in the geodetic sites LOGO, LEON, OMAL, ROML and KAPT; (3) along the Arabian boundary zero velocities are assumed (white triangles in Fig. 1a); and (4) along the eastern boundary of the model, shear-stress-free conditions are assumed (white circles in Fig. 1a). For further details about the motivations for these boundary conditions, we refer the reader to the original paper, Marotta *et al.* (2004).

The boundary conditions along the southern boundary of the model account for Africa–Eurasia relative motion based on ITRF2005 (Altamimi *et al.* 2007) (black triangles in Fig. 1a) and are calculated following the procedure in Nocquet *et al.* (2001) to estimate the Eulerian Pole. The geodetic stations PENC, BOR1, BRUS, VILL, ZIMM, POTS, HERS, TOUL, MADR and YEBE (black circles in Fig. 2) define the stable Europe (Devoti *et al.* 2002), and GOUG, SUTH, MAS1 (white circles in Fig. 2) define the stable Africa (McClusky *et al.* 2003).

Table 1 lists the models considered in the analysis.

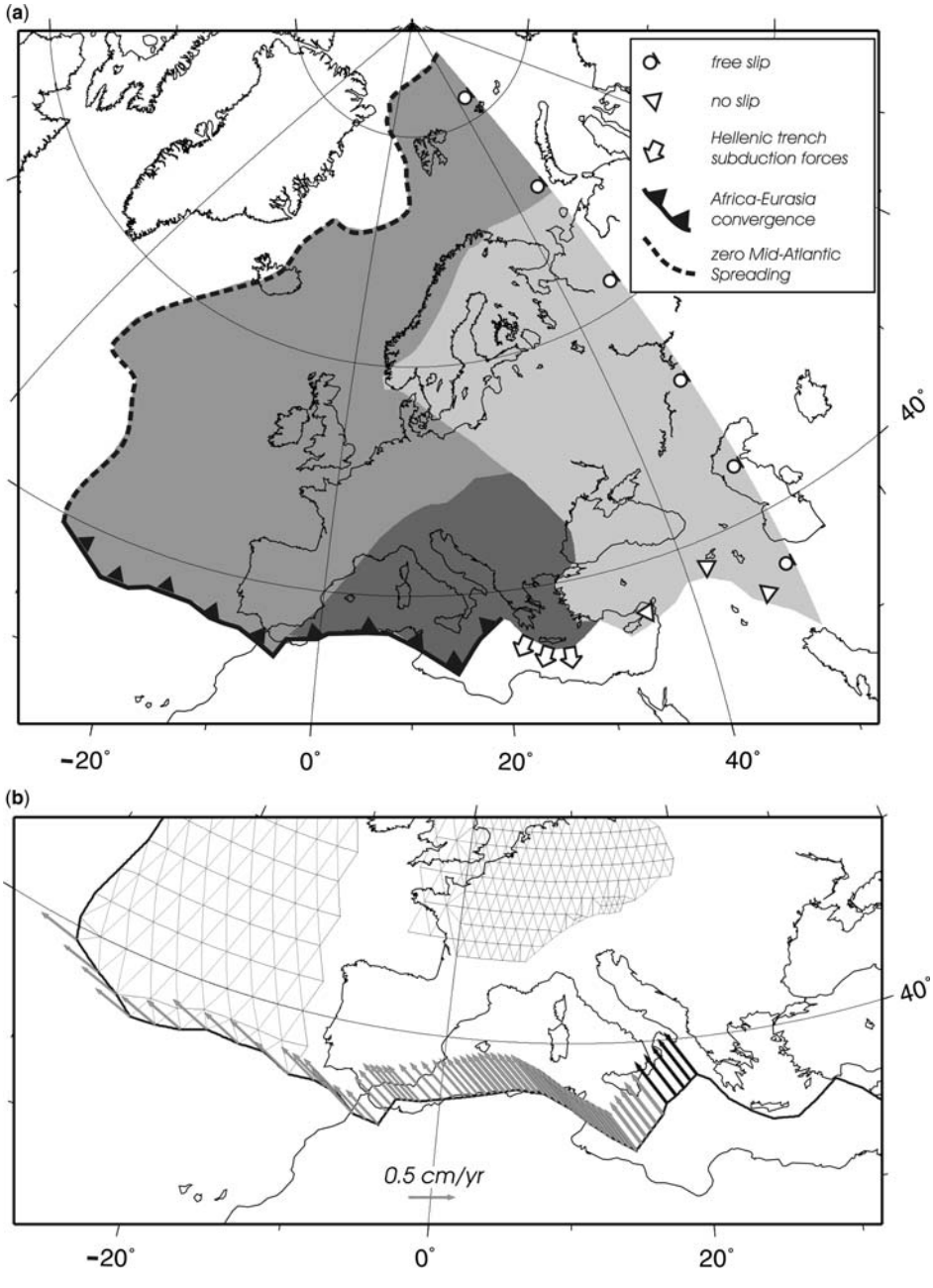


**Fig. 1.** (**a**) Geometry and boundary conditions of the domain where the 2D numerical analysis has been performed. The study area is composed of three major blocks: the East European platform (light grey); the European domain (intermediate grey); and the Mediterranean (dark grey). The black triangles reflect the counterclockwise rotation of the African plate with respect to the European plate that is calculated in this study on the base of the ITRF2005 velocity solutions. Along all of the other boundaries the assumed boundary conditions are the same as the best-fit model of Marotta *et al.* (2004): zero Mid-Atlantic spreading (dashed thick black line); shear-stress-free conditions along the eastern boundary of the study domain (white circles); no-slip conditions along the southern boundary of the Anatolian region (white triangles); velocity along the Aegean trench based on McClusky *et al.* (2000) (white arrows). (**b**) Details of the 2D numerical grid used for the analysis. The arrows indicate the Africa–Eurasia convergence velocities as calculated in the present study along the SW portion of the study domain. See the text for further details.


**Fig. 2.** Position of the IGS stations used in the geodetic analysis (white stars) and of the geodetic stations used to define stable Europe (black circles) and stable Africa (white circles) in the calculation of the Africa–Eurasia relative motion.

**Table 1.** *List of the models considered in the present analysis*

| Model | Reference strain rate ($s^{-1}$) | TM | Block | Convergence percentage (%) |
|---|---|---|---|---|
| Block_100% | – | | x | 100 |
| Block_75% | – | | x | 75 |
| Block_50% | – | | x | 50 |
| Block_25% | – | | x | 25 |
| Block_0% | – | | x | 0 |
| TM16_100% | $10^{-16}$ | x | | 100 |
| TM16_75% | $10^{-16}$ | x | | 75 |
| TM16_50% | $10^{-16}$ | x | | 50 |
| TM16_25% | $10^{-16}$ | x | | 25 |
| TM16_0% | $10^{-16}$ | x | | 0 |
| TM19_100% | $10^{-19}$ | x | | 100 |
| TM19_75% | $10^{-19}$ | x | | 75 |
| TM19_50% | $10^{-19}$ | x | | 50 |
| TM19_25% | $10^{-19}$ | x | | 25 |
| TM19_0% | $10^{-19}$ | x | | 0 |

### *Lithosphere temperature*

The thermal analysis is based on a 3D numerical model performed in the central Mediterranean (dark grey in Fig. 1a). The steady-state 3D thermal field is calculated by integrating the energy equation:

$$\nabla \cdot (k\nabla T) + \rho H = 0 \tag{3}$$

on a 3D grid composed of prismatic elements obtained by projecting along the depth the 2D numerical grid used in the tectonic model (Fig. 3a). $K$ is the thermal conductivity, $T$ is the temperature, $\rho$ is the density and $H$ the rate of radiogenic heat production per unit mass. The model accounts for crust (dry felsic granulite) and mantle (dry dunite) up to a depth of 200 km (Fig. 3b). Parameter values are listed in Table 2.

Dirichlet boundary conditions are prescribed at the upper boundary of the model, with the temperature fixed to 300 K. Neumann boundary conditions are prescribed at the lower boundary of the model, where the assumed heat flow coincides with the residual heat flow, $q_r$, derived from the observed surface heat flow, $q_s$ [Pollack *et al.* 1993, augmented by Artemieva's (2006) data] through the Pollack & Chapman (1977) formula:

$$q_r = 0.6q_s. \tag{4}$$

Zero heat flow is prescribed at the vertical sides of the model.

The upper surface and the base of the crust are defined by interpolating the topography and the Moho depth from Bassin *et al.* (2000) at the nodes of the 3D numerical grid. While the base of the crust is physically defined, the base of the lithosphere is defined thermally by the isotherm 1600 K resulting from the integration of equation (3) with the above specified boundary conditions.

## Lithosphere strength

The lithosphere strength is calculated by assuming that rocks behave like a brittle or ductile material according to their composition and thermal state.

For the brittle behaviour, a linear failure criterion is assumed (Ranalli & Murphy 1987), as expressed for the dry rheology assumed in the present analysis in the form:

$$\sigma_B = (\sigma_H - \sigma_V)_B = \beta r \rho g \tag{5}$$

where $r$ is the depth along the terrestrial radius, $\rho$ is the density of the material (2800 kg m$^{-3}$), $g$ is the acceleration of gravity, and $\beta$ a parameter depending on the type of faulting and assumed to be equal to 3 for thrust faulting, 1.2 for strike-slip faulting and 0.75 for normal faulting (Ranalli & Murphy 1987).

Ductile behaviour is controlled by the power law (Weertman & Weertman 1975):

$$\sigma_D = (\sigma_H - \sigma_V)_D = \left(\frac{\dot{\varepsilon}}{\dot{\varepsilon}_0}\right)^{\frac{1}{n}} \exp\left(\frac{E_a}{nRT}\right) \tag{6}$$

where $\dot{\varepsilon}$ is the strain rate, and ranges between $10^{-19}$ and $10^{-16}$ s$^{-1}$; $R$ is the universal constant of gas, $T$ is the absolute temperature, and $\dot{\varepsilon}_0$, $n$ and $E_a$ are constant characteristics of the rocks (Table 2).

The strength envelope for each type of faulting is determined as:

$$\sigma_y = \min\{\sigma_B, \sigma_D\} \tag{7}$$

and the effective viscosity at each element of the 2D numerical grid as:

$$\mu_{eff} = \frac{1}{\dot{\varepsilon}} \frac{1}{L} \int_0^L \sigma_y \, dy \tag{8}$$

where $L$ is the thickness of the thermal model.

## Data

### *Crustal thickness*

Figure 4 shows the crustal thickness variation used in the thermal and tectonic analysis for the Mediterranean and central Europe, based on the CRUST 2.0 model (Bassin *et al.* 2000). The area is characterized by strong lateral variation with a thin crust in the Provencal Basin, Tyrrhenian Basin and north of the Pannonian Basin. A thick crust characterizes the Alps, the north of the Adriatic Sea and the Ellenic arc.

### *Heat flow*

Figure 5 shows the surface heat flow used in the thermal analysis, obtained by interpolating onto the 2D numerical grid the discrete database of Pollack *et al.* (1993), augmented by Artemieva (2006) in the areas with no data. Black circles indicate the data of Pollack *et al.* (1993). The thin southern Tyrrhenian is characterized by rather high values of surface heat flow, higher than 100 mW m$^{-2}$, as occurs also in the north of the Pannonian Basin. Rather low values of heat flow characterize the north Adriatic and the Ionian Sea. Owing to the regional character of the present study, the

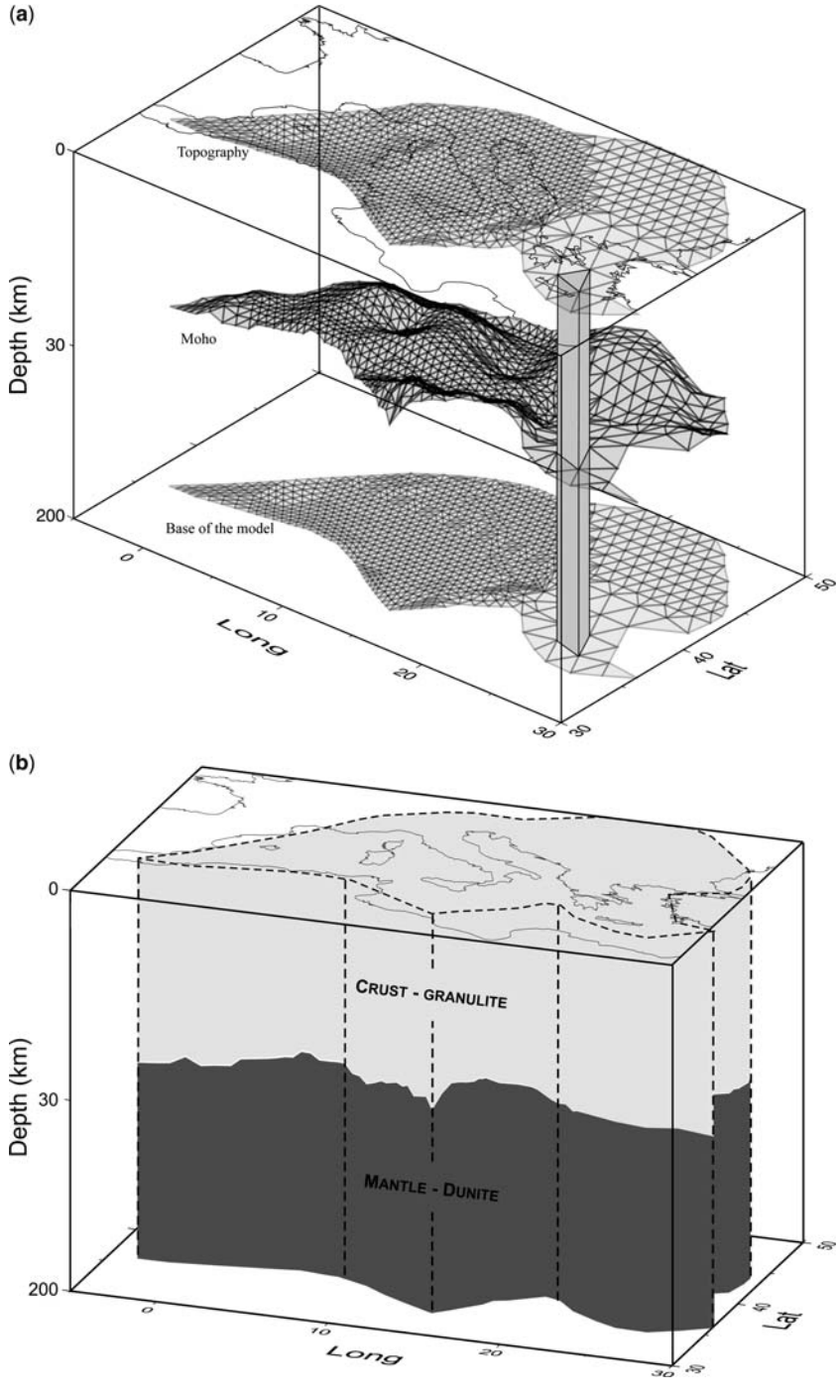


**Fig. 3.** (**a**) Scheme of the 3D numerical grid used for the thermal analysis. The assumed linear prismatic elements are obtained by projecting the 2D grid along the depth. The vertical axis is not to scale. (**b**) Structural sketch of the 3D model.

**Table 2.** *List of the parameters used in the thermorheological analysis*

| | Lithology | $\dot{\varepsilon}_0$ ($Pa^{-n} s^{-1}$) | $n$ | $E_a$ ($j\ mol^{-1}$) | $\rho$ ($kg\ m^{-3}$) | $H$ ($W\ kg^{-1}$) | $K$ ($W\ m^{-1}\ K^{-1}$) |
|---|---|---|---|---|---|---|---|
| Crust | Dry felsic granulite | $20.095 \times 10^{-22}$* | 3.1* | $243 \times 10^{3}$* | 2800 | $7.5 \times 10^{-10}$ | 2.55 |
| Mantle | Dry dunite | $6.310 \times 10^{-17}$† | 3.41† | $444 \times 10^{3}$† | 3200 | $6.3 \times 10^{-13}$ | 4.15 |

*Afonso & Ranalli (2004); †Chopra & Peterson (1981).
$\dot{\varepsilon}_0$, exponent of the power-law creep equation; $n$, pre-exponential factor of the power-law creep equation; $E_a$, activation energy.

extremely high values of heat flow observed in the Larderello (450–700 mW $m^{-2}$) and Stromboli (250–822 mW $m^{-2}$) areas have been filtered before the interpolation.

### *Stress data*

Numerical results will be discussed in terms of predicted velocities and tectonic deformation. In this last aspect, the most recent World Stress Map 2008 compilation (Heidbach *et al.* 2008) offers new insights on the present-day enigmatic regional deformation pattern characterizing the Tyrrhenian area. Figure 6 shows the maximum principal horizontal stresses in the study area, highlighting areas subjected to extension (white bars) within the regional context of active Africa–Eurasia convergence.

### *The geodetic dataset*

Continuous GPS (CGPS) data of the most long-lived permanent stations in the surroundings of the Calabrian Arc have been taken into account to compare the tectonic regional deformation model with geodetic observations. The geodetic network consists

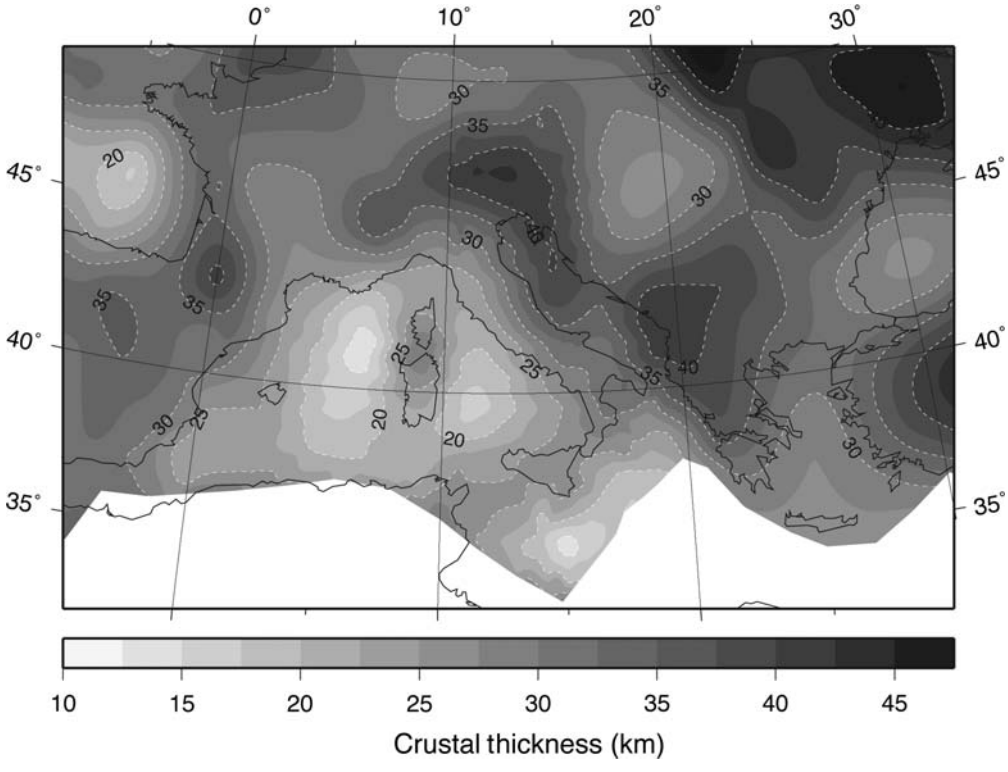


**Fig. 4.** Crustal thickness variation used in both the thermal and mechanical analyses, and obtained by linear interpolation onto the adopted grid of model CRUST 2.0 (Bassin *et al.* 2000).

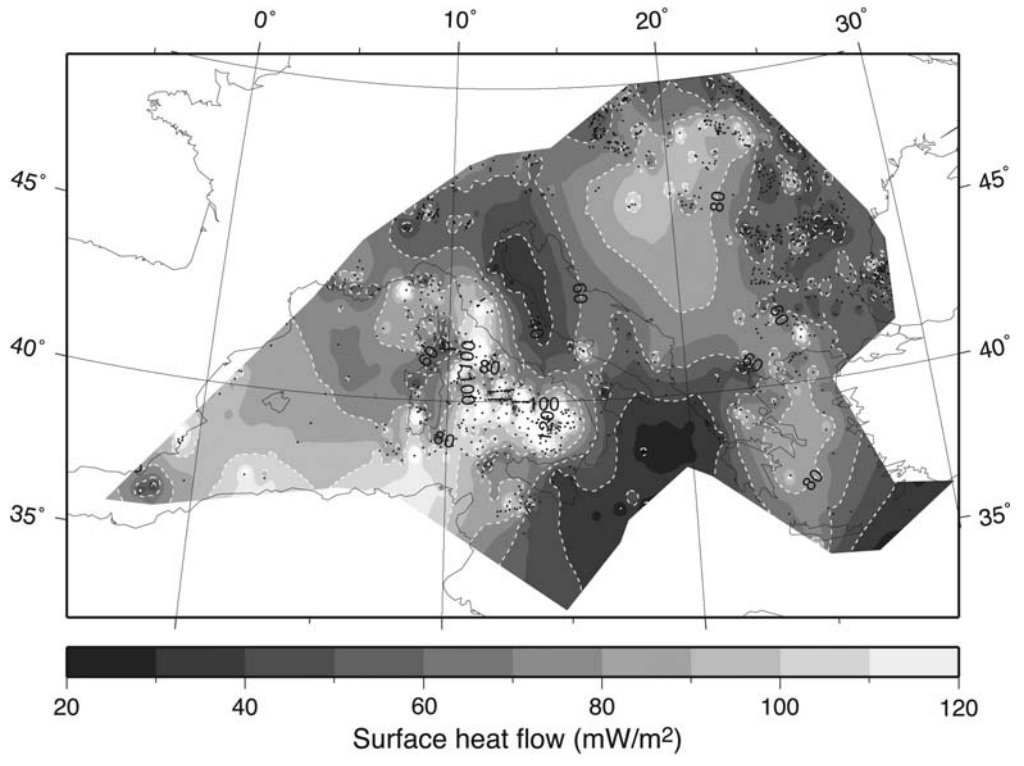


**Fig. 5.** Surface heat flow variation used in the analysis and obtained by linear interpolation onto the adopted grid of Pollack *et al.* (1993), augmented by the database of Artemieva (2006). Black circles represent the original data of Pollack *et al.* (1993).

of 15 permanent GPS stations, which are plotted in Figure 7. For these stations, daily co-ordinate time series have been estimated; they span a variable year number, ranging from almost 10 years to a minimum of 3 years.

The GPS data analysis has been carried out with BERNESE Software v.5.0 (Dach *et al.* 2007), using a standard processing strategy: troposphere parameters have been estimated on an hourly basis and wet delays have been modelled as stochastic parameters using the Dry-Niell mapping function; the ionosphere disturbance has been treated using global ionosphere models by CODE (Hugenobler *et al.* 2000) in the L1&L2 ambiguity estimation step and using the iono-free observations (L3) in the co-ordinate computation. The Quasi Iono Free (QIF) strategy was selected for ambiguity fixing. According to the IGS (International GNSS Service) standard, absolute PCV (Phase Centre Variation) parameters have been used both for receiver and satellite antennas.

The reference frame of the daily co-ordinates is consistent with IGS precise orbits and IGS Earth rotation parameters. The IGS stations used to fix the frame are WTZR, ZIMM, GRAS, VILL, NICO, EBRE and ANKR (white stars in Fig. 2) depending on the current reference frame realization. Station co-ordinates have all been framed in IGS05 using the IGS transformation parameters at the end of the processing analysis.

The velocity estimation (empty arrows in Fig. 7) has been determined by least-square adjustment of individual daily co-ordinate components; the applied functional model consists of linear trends and periodic components (Blewitt & Lavallée 2002; Dong *et al.* 2002; Nikolaidis 2002; Ray *et al.* 2008). Possible discontinuities owing to reference frame or antenna–receiver changes have also been estimated and reduced.

The noise characteristics of the GPS time series have been studied following the Empirical Covariance Function method, as described in Cannizzaro (2008).

Black arrows in Figure 7 indicate the same velocity solutions once they have been transformed into the reference frame of the geophysical models.

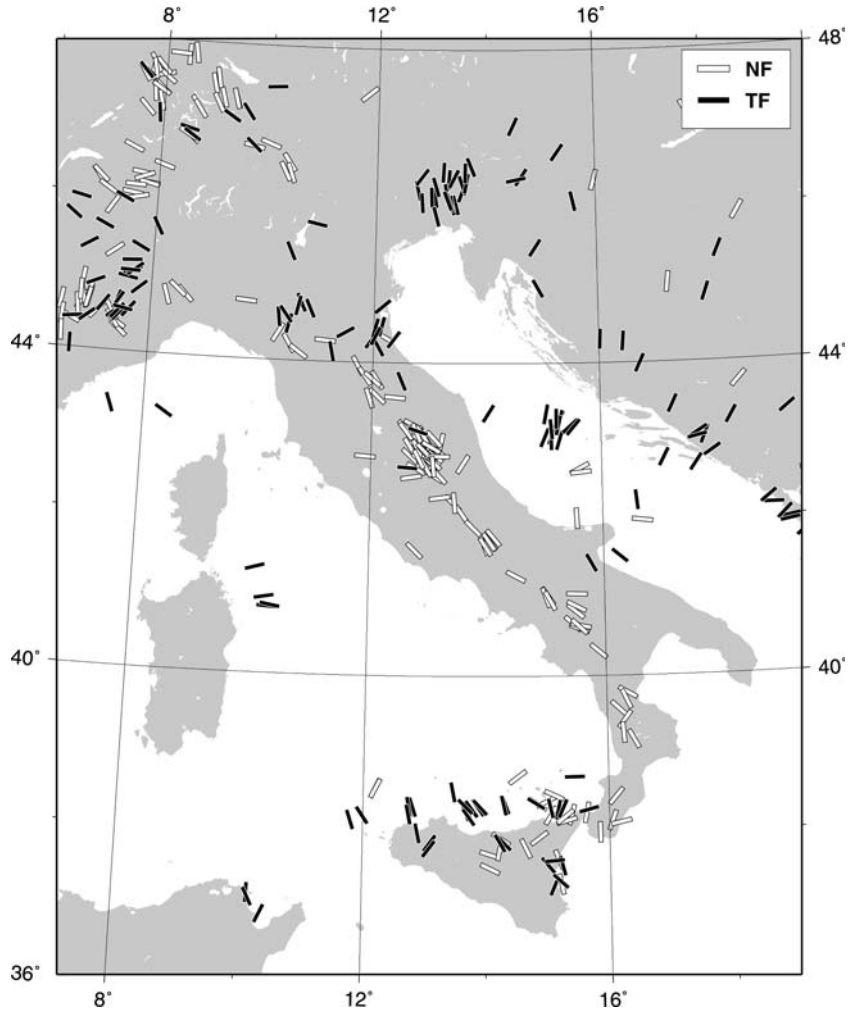


**Fig. 6.** Maximum principal horizontal stresses in the Italian Peninsula, based on the World Stress Map 2008 compilation (Heidbach *et al.* 2008). NF, normal faulting; TF, thrust faulting.

## Results and discussion

### *Lithosphere temperature*

The lithosphere thermal field predicted in the study area is represented in Figure 8, where the temperature at the base of the crust (Fig. 8a) and the depth of the 1600 K isotherm, assumed to be the base of the thermal lithosphere (Fig. 8b), are shown. It is worth noting the different pattern of the thermal field at the crustal and lithosphere levels. Concerning the temperature at the base of the crust (Fig. 8a), steep gradients are observed throughout the study area, with low temperatures (less than 900 K) predicted at the base of the thin Tyrrhenian crust, and high temperatures (greater than 1000 K) predicted east of the Apennine. Conversely, smooth variations characterize the depth of the base of the lithosphere (Fig. 8b), with an average lithosphere thickness (neglecting the topography) ranging between 70 and 90 km. The strongest gradients occur south of the Calabrian Arc, in proximity to the trench associated with the Calabrian subduction, where a thermal doubling occurs within 500 km.

### *Lithosphere strength*

The predicted 3D lithosphere thermal field is used to determine the strength of the lithosphere in the Mediterranean region, according to (5)–(7). For

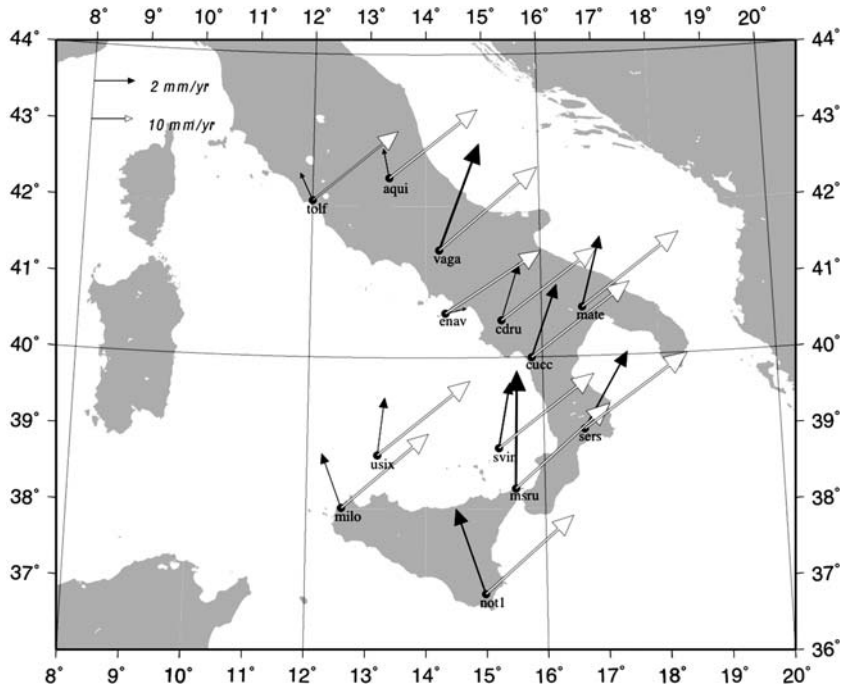


**Fig. 7.** Geodetic velocity solutions (white arrows) at the permanent stations MATE, NOT1, AQUI, MILO, MSRU, USIX, SVIN, SERS, CUCC, CDRU, ENAV, LAMP, MALT, VAGA and TOLF, obtained by analysing their daily position solutions. Black arrows indicate the same solutions after their transformation into the reference frame of the geophysical models.

ductile behaviour, dry felsic granulite is assumed for the crust and dry dunite is assumed for the lithospheric and sublithospheric mantle (Table 2). Figure 9 shows the vertical strength envelopes at six reference sites distributed in the study area (A–F in Fig. 8a) obtained for two reference values of the strain rate ($10^{-16}\,s^{-1}$, right-hand side, and $10^{-19}\,s^{-1}$, left-hand side, of each panel), and for thrust (dark grey), normal (light grey) and strike-slip (intermediate grey) faults. The black dashed lines represent the corresponding vertical temperature profiles.

In agreement with the thermal field, a strong lithosphere paves the Tyrrhenian, with a strong coupling between crust and mantle at the Provencal Basin (site A, Fig. 9a) and south of the Calabrian Arc (site C, Fig. 9c). A relatively softer lithosphere characterizes the Marsili Basin (site B, Fig. 9b) north of the Calabrian Arc, where a local thermal rise occurs. Lithosphere strength profiles predicted at sites D–F (Fig. 9d–f, respectively) are almost coincident. The concurrence of hot lithosphere and thick crust in the eastern portion of the model drives an average soft lithosphere, with a negligible mantle contribution to the total strength as a peculiar feature.

The effective lithosphere viscosity results from the integration of the vertical strength envelopes. For a given lithosphere thermal field, three elemental distributions of effective viscosity are obtained, corresponding to the three types of faulting regime. Thus, Figure 10 shows the variation of lithosphere effective viscosity for thrust (panels $a_i$), strike-slip (panels $b_i$) and normal (panels $c_i$) regimes, and for the two values of reference strain rate, $10^{-19}\,s^{-1}$ (panels $a_1$, $b_1$ and $c_1$) and $10^{-16}\,s^{-1}$ (panels ($a_2$, $b_2$ and $c_2$). Changing the reference strain rate from $10^{-19}$ to $10^{-16}\,s^{-1}$ induces a global lithospheric softening of almost 3 orders of magnitude.

Each tectonic model initially assumes the effective viscosity distribution to be that corresponding to strike-slip faulting; then, it iterates and progressively changes the effective viscosity of each element according to its new strain regime. Figure 11 shows the effective viscosity predicted in the central Mediterranean by a model accounting for reference strain rates of $\dot{\varepsilon} = 10^{-16}\,s^{-1}$ (Fig. 11a) and $\dot{\varepsilon} = 10^{-19}\,s^{-1}$ (Fig. 11b). In both cases the Apennine defines a transition from a relatively soft lithosphere, extending from the eastern Alps through to the Pannonian Basin, to a stiffer

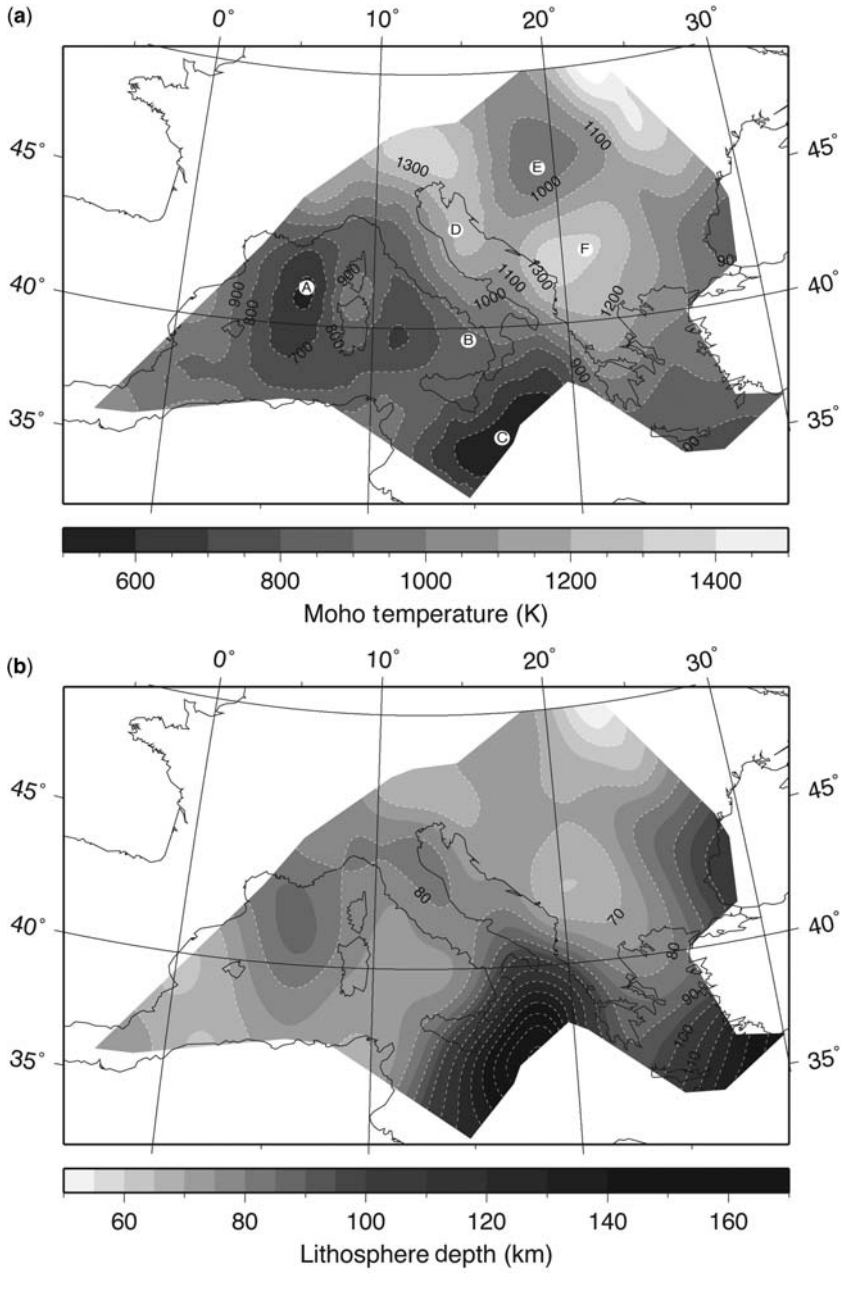


**Fig. 8.** (**a**) Predicted temperature at the Moho depth. (**b**) Predicted depth of the 1600 K isotherm (assumed base of the thermal lithosphere). Capital letters in panel (a) indicate the six sites where the strength envelopes shown in Figure 9 are calculated.

lithosphere, below the Tyrrhenian Sea, where changes of up to 1.5 orders of magnitude occur in the effective viscosity. At shorter wavelengths our rheological analysis supports the rheological differentiation between north and south Adria (e.g. Oldow *et al.* 2002), with, in our case, the northern block stiffer by about half an order of magnitude than the southern one (Fig. 11a).

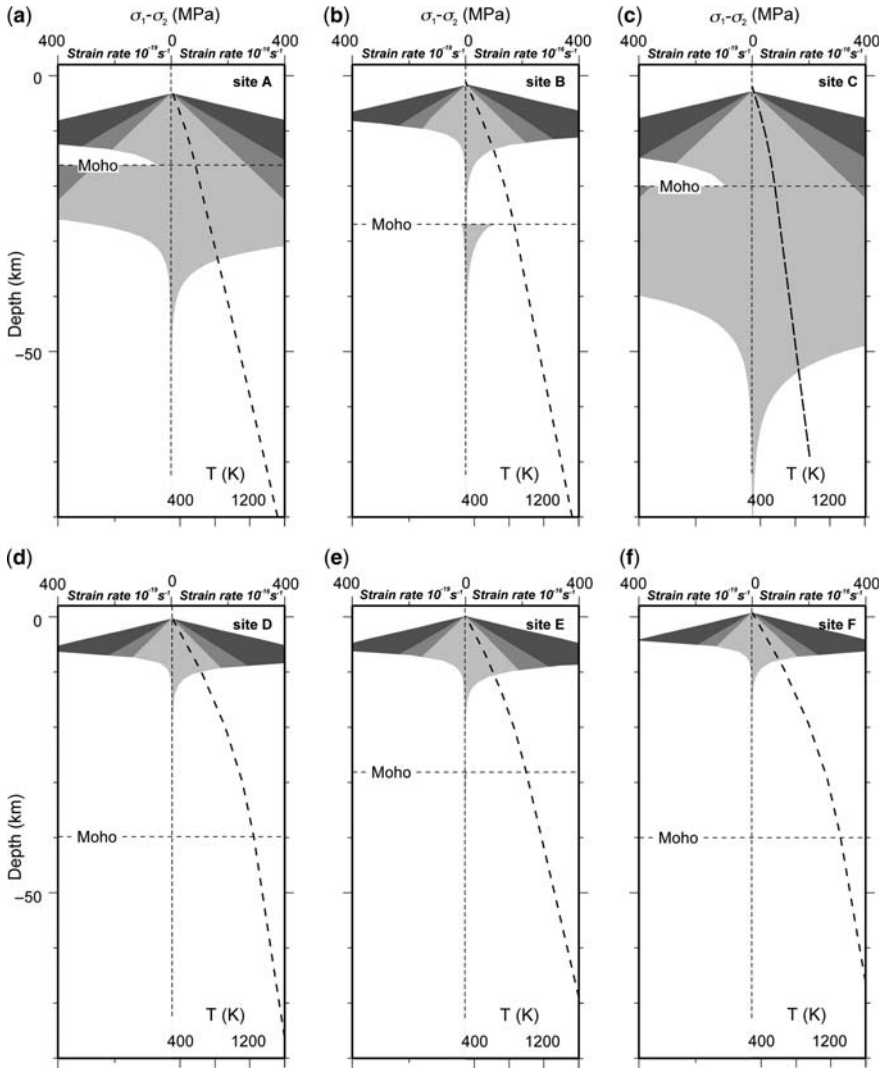


**Fig. 9.** Predicted lithosphere strength envelopes at the six sites shown in Figure 8a obtained assuming a reference strain rate of $10^{-16}$ s$^{-1}$ (right-hand side of each panels) or $10^{-19}$ s$^{-1}$ (left-hand side of each panel), and for thrust (dark grey), normal (light grey) and strike-slip (intermediate grey) faults. Black dashed lines represent the corresponding vertical temperature profiles.

## *Tectonic deformation*

Figure 12 compares the strain rate predicted by tectonic model TM16 using the effective viscosity of Figure 11a to the tectonic strain rate predicted by an equivalent tectonic block model in which a rheologically uniform lithosphere is assumed below the Mediterranean, with an effective viscosity of $10^{25.5}$ Pa s (Fig. 11b). The block model predicts compression through the study area, with the strongest gradients localized along a longitudinal stripe between 37° and 40° of latitude and dominant SE–NW eigen-directions (Fig. 12b), according to the Africa–Eurasia convergence direction. Rather small and uniform deformation is predicted at the higher latitudes. Similar to the block model, the TM16 model predicts compression at intermediate latitudes; however, the lateral rheological heterogeneities concur with the variation in lateral crustal and lithosphere thicknesses to induce strong lateral gradients in the deformation field that also shows strong compression at the high

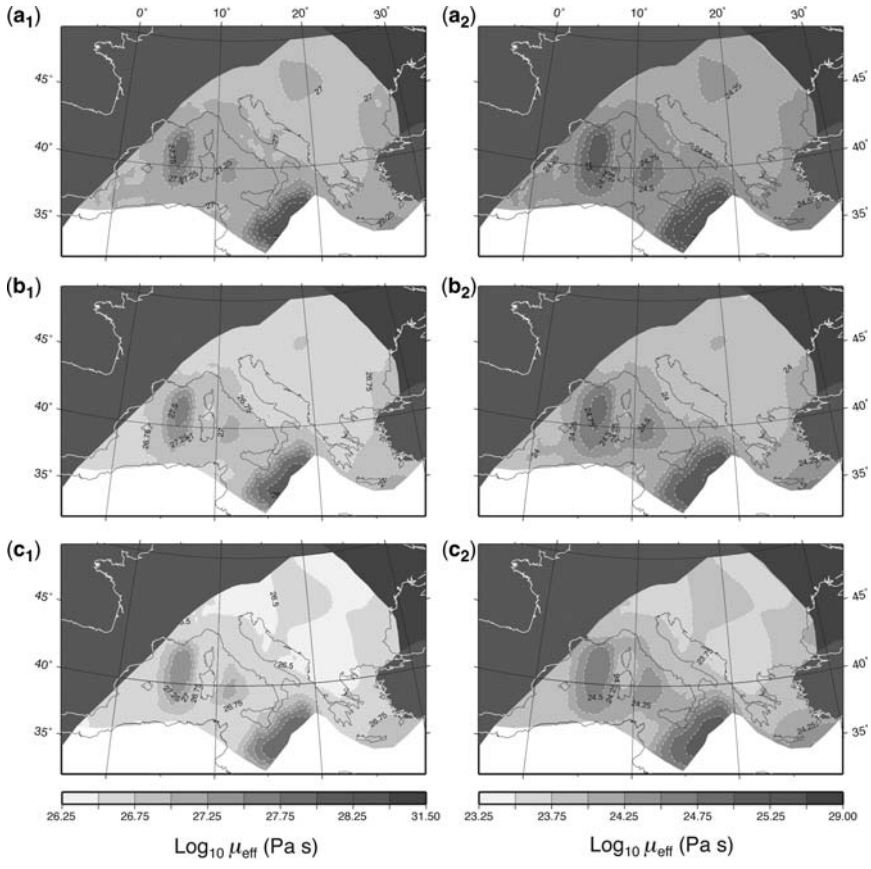


**Fig. 10.** Variation of lithosphere effective viscosity obtained for the thrust (panels $a_i$), strike slip (panels $b_i$) and normal (panels $c_i$) regime, and for a reference strain rate of $10^{-19}$ $s^{-1}$ (panels $\mathbf{a}_1$, $\mathbf{b}_1$ and $\mathbf{c}_1$) and $10^{-16}$ $s^{-1}$ (panels ($\mathbf{a}_2$, $\mathbf{b}_2$ and $\mathbf{c}_2$).

latitudes. Furthermore, a slight counterclockwise rotation of the compressive component of the strain-rate eigenvectors occurs at the intermediate latitudes. Another peculiar feature that differentiates the deformation patterns predicted by the two models is the diffuse SW–NE extension, as intense as the compression, predicted by the TM16 model in the region below 38° of latitude (Fig. 11a). This last result is in agreement with the evidence of extension within the regional context of active Africa–Eurasia convergence, as evidenced by the World Stress Map 2008 compilation (Fig. 6).

Despite these promising results, the TM16 model has the tendency to underestimate the extensional component of the strain-rate tensor, in particular at the intermediate latitudes. Trying to overcome this limitation and to improve, in particular, the extension in the southern Tyrrhenian, we embrace Marotta & Sabadini's (2008) hypothesis that partially ascribes the underestimation of the extension to the absence of subduction in the thin-sheet tectonic model. We therefore implement new models in which only 75, 50, 25 and 0% of the estimated Africa–Eurasia convergence is transmitted to the Eurasian plate through the Calabrian subduction zone. Numerically, this corresponds to a progressive decrease in the magnitude of the prescribed velocities at the nodes of the numerical grid delimiting the Calabrian trench, represented by the black arrows in Figure 1b.

Figure 13 shows the deformation pattern predicted by the model TM16_50, using 50% of Africa–Eurasia convergence. This model moves the extension–compression interface further to the north, and enhances extension throughout Sicily and south of Calabria. Furthermore, a SE–NW compression appears in the Algerian region, as indicated by the World Stress Map 2008 (Heidbach *et al.* 2008).

TM16_50 is the model that best reproduces the regional tectonic deformation in the Mediterranean; this role is also demonstrated by a direct comparison

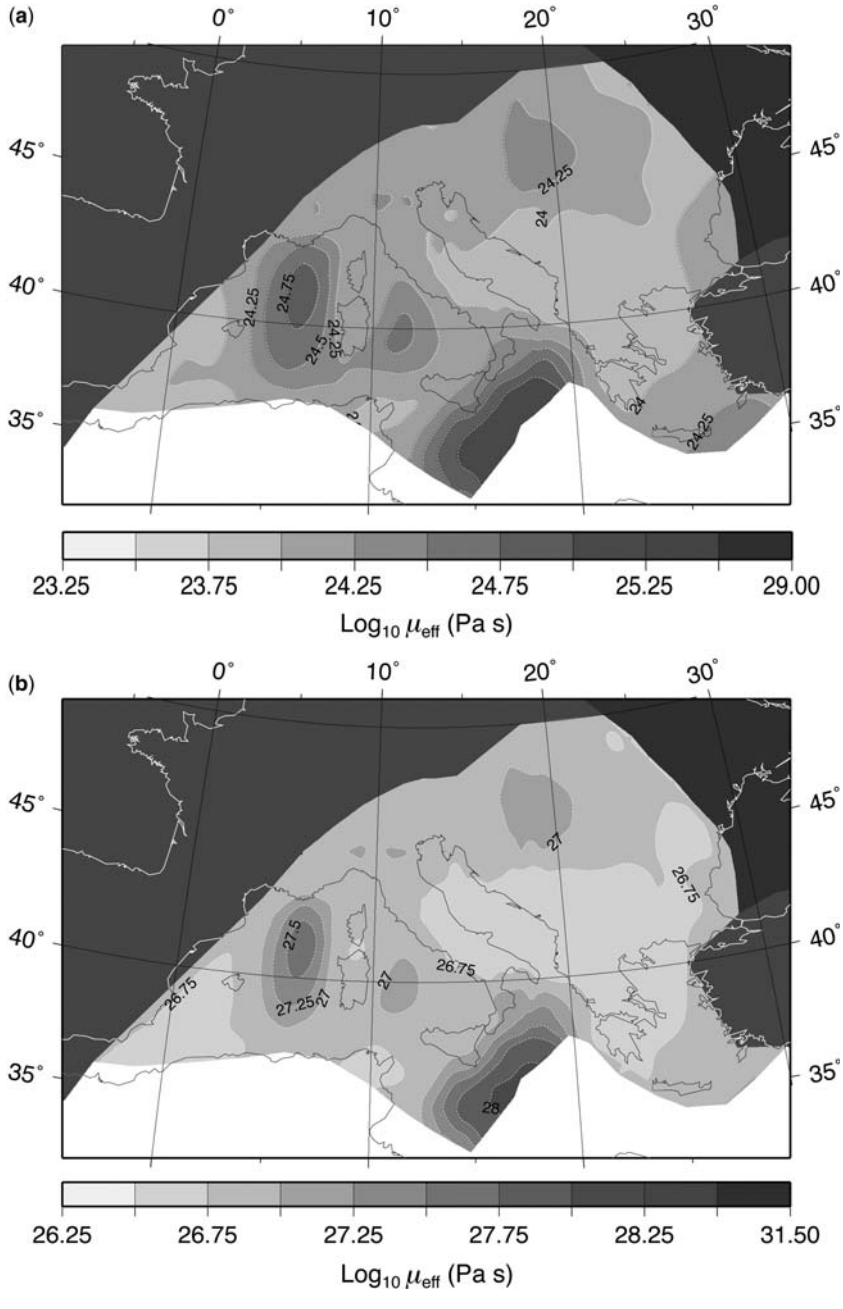


**Fig. 11.** Effective viscosity predicted for a reference strain rate of (**a**) $10^{-16}$ $s^{-1}$ and (**b**) $10^{-19}$ $s^{-1}$.

between observed and predicted velocities at 15 permanent geodetic stations distributed around the Calabrian Arc. Predicted velocities (coloured arrows) for all the analysed models of Table 1 are shown in Figure 14 compared to the velocities from the geodetic measurements (black arrows). One major comment is that all of the block-type models predict velocities apparently in great disagreement with the geodetic velocities, both in magnitude and azimuth (Fig. 14a). The fit from the block model gets worse with the progressive decreasing of the per cent of Africa–Eurasia convergence allowed

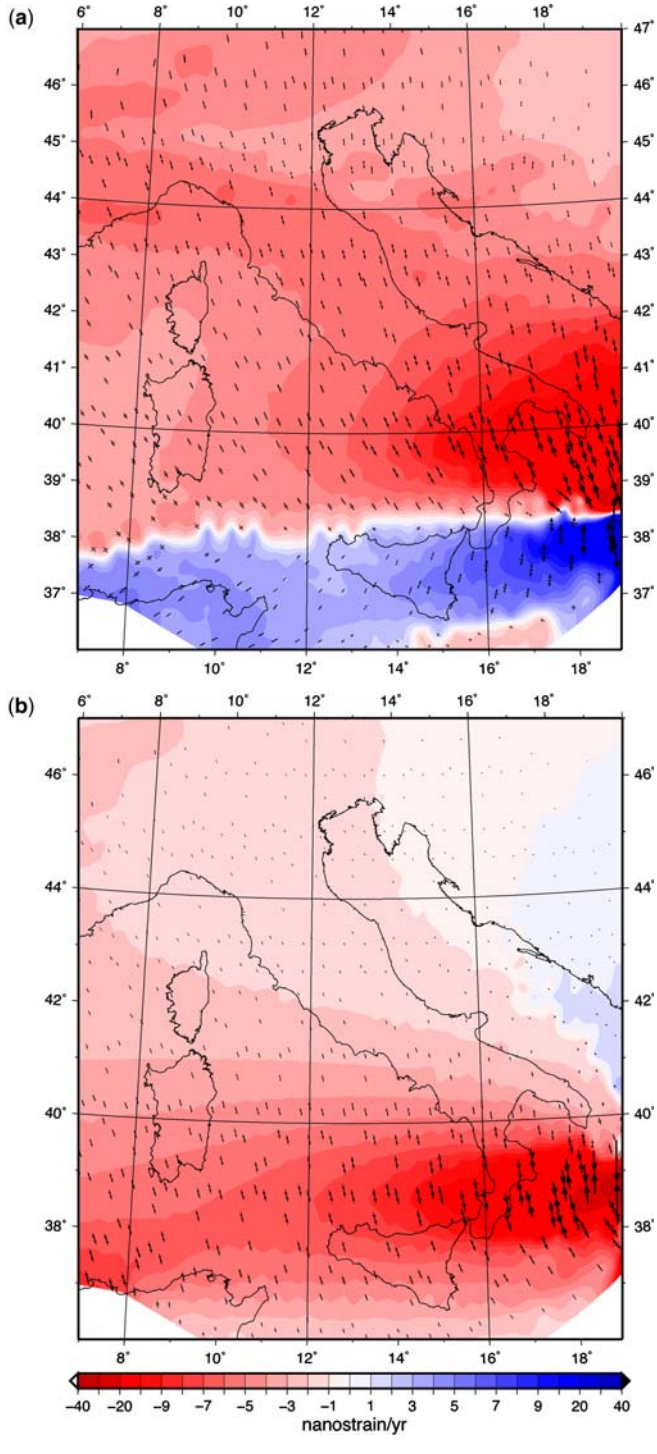


**Fig. 12.** Strain-rate regime (colour map, with red indicating compression and blue extension) predicted by (**a**) model TM16 and the (**b**) block model, including 100% of the Africa–Eurasia convergence transmitted to the Eurasian plate through the Calabrian subduction zone.

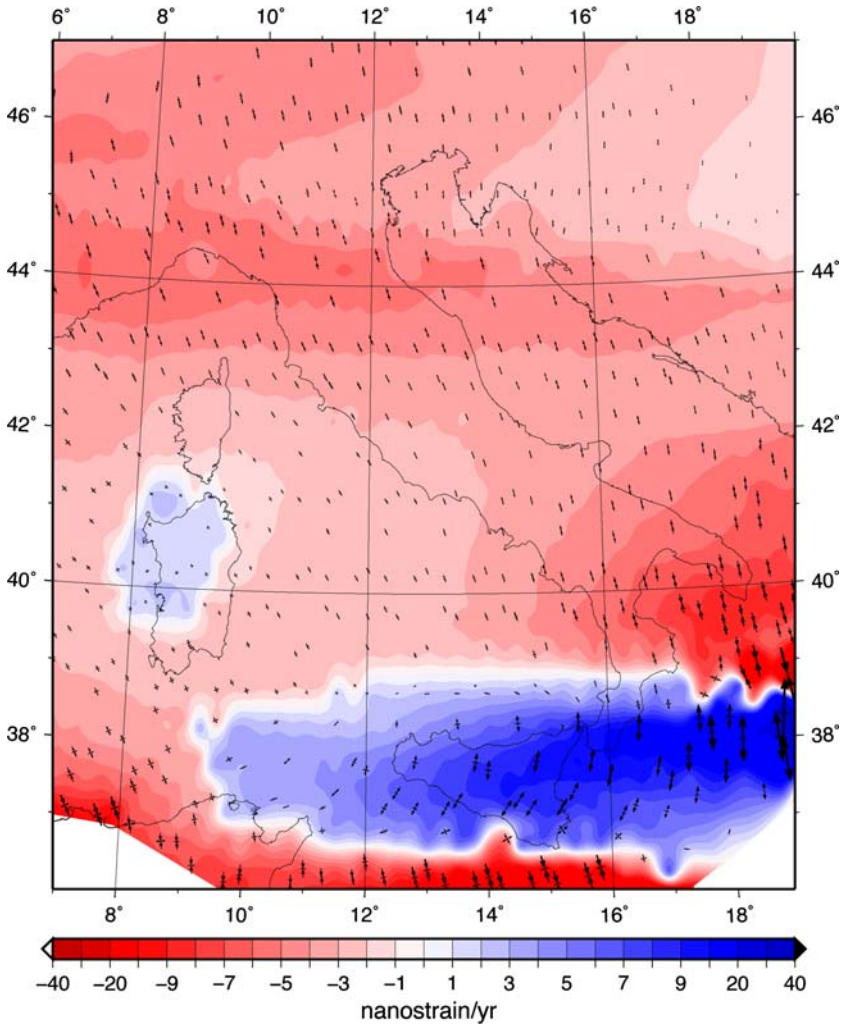


**Fig. 13.** Strain-rate regime (colour map, with red indicating compression and blue extension) predicted by model TM16_50, including 50% of the Africa–Eurasia convergence transmitted to the Eurasian plate through the Calabrian subduction zone.

to be transmitted through the Calabrian subduction; this induces a progressively larger disagreement, in both magnitude and azimuth, of the predicted velocities and the GPS velocities. Models that take into account the temperature dependence of viscosity show a better agreement in magnitude (e.g. at AQUI and MATE) and a greater variation in the azimuth with the variation of the per cent of Africa–Eurasia convergence transmitted through the Calabrian subduction, which makes model TM16_50% the best-fitting model.

This conclusion is further strengthened by a $\chi^2$ analysis. As the CGPS velocities have been estimated for each component of each station independently, the quadratic form of the $n$ normalized horizontal velocity residuals is chi-square distributed, with $n$ degrees of freedom,

$$\mathbf{U}^{+}\mathbf{C}^{-1}\mathbf{U} = \chi_n^2$$

where $\mathbf{U}$ is an $n$-dimensional vector formed by the difference values between the horizontal GPS velocities ($v_{\mathrm{N}}$, $v_{\mathrm{E}}$) after a datum shift to ITRF2005 and geophysical model velocities, and $\mathbf{C}$ is the diagonal matrix containing the velocity variances.

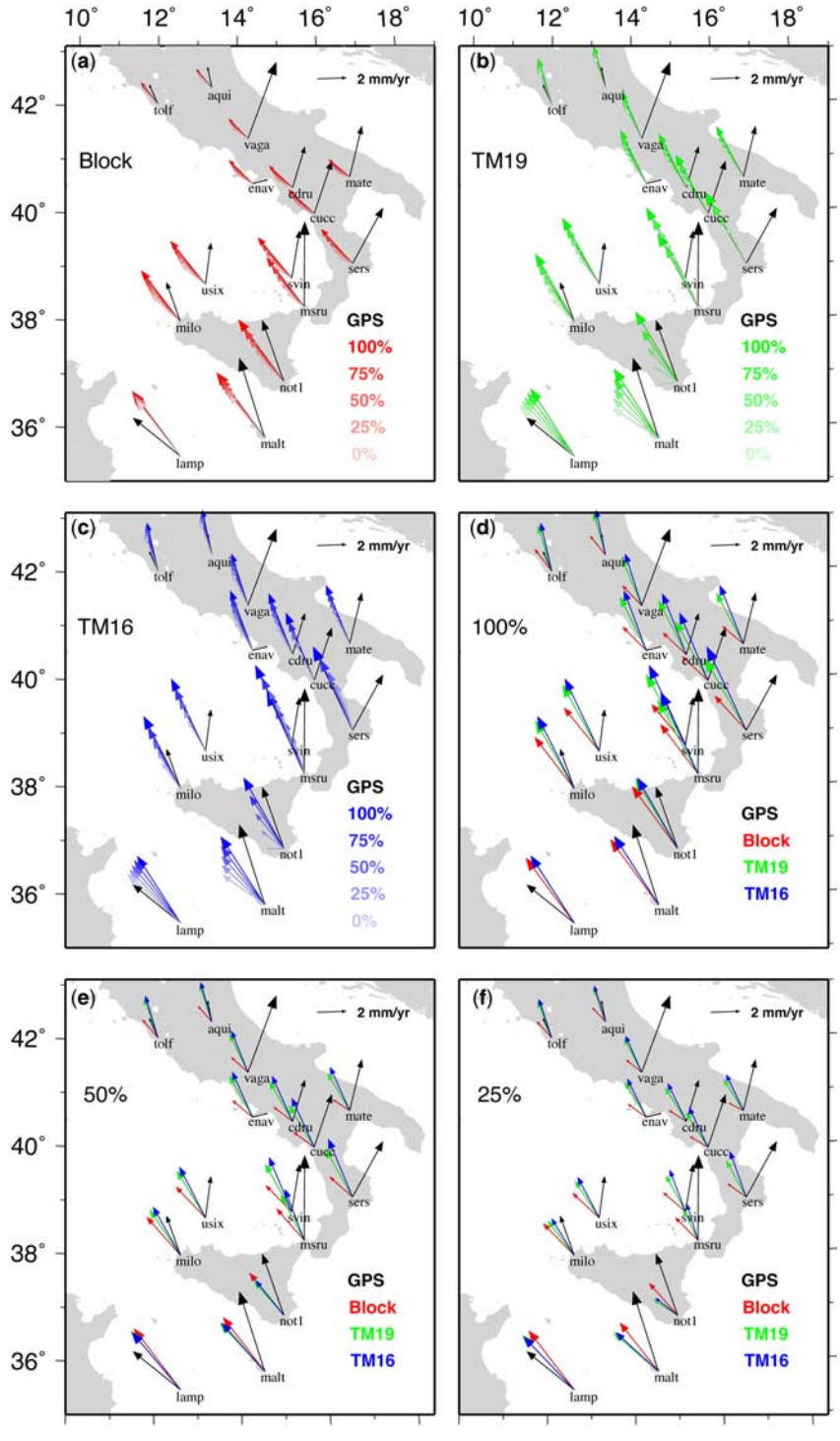


**Fig. 14.** Predicted (coloured arrows) v. GPS velocities (black arrows). The per cent represents the amount of Africa–Eurasia convergence transmitted through the Calabrian subduction.

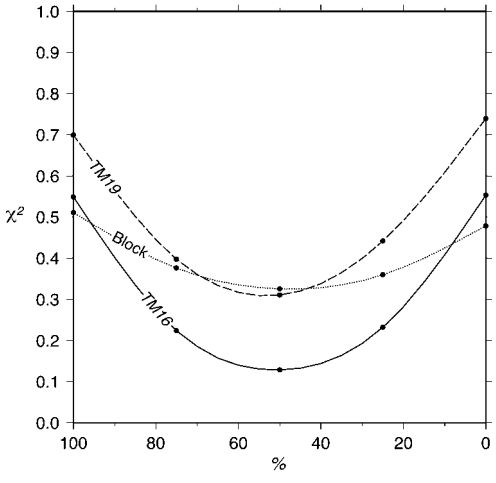


**Fig. 15.** Classification of the geophysical models obtained with the $\chi^2$ analysis. The per cent indicates the percentage of the Africa–Eurasia convergence transmitted to the Eurasian plate through the Calabrian subduction zone.

The geophysical models are qualitatively classed by using this statistic; the lower the $\chi^2$ value, the better the agreement between the tested model and the geodetic data. Figure 15 shows the final classification of all the geophysical models using the statistic $\chi^2$ test. A first general observation can be made by focusing on the effects of a local reduction of the convergence due to Calabrian subduction; the lower the percentage, the better the agreement between model and observation. The block-type model shows the best agreement with the data only when 100% of Africa–Eurasia convergence is included. A decrease in the per cent of Africa–Eurasia convergence transmitted through the Calabrian subduction does not significantly affect the block model, as shown in Figure 14a and Figure 15 (dotted line). The model that exhibits the best agreement with observation is the TM16_50 model, in which the assumed effective viscosity is obtained from a reference strain rate of $10^{-16}$ s$^{-1}$ and 50% of Africa–Eurasia convergence is transmitted though the Calabrian Arc. From about 95% on the thermomechanical model TM16 is the best-fit model, within any configuration. Note the poor quality of thermomechanical model TM19; it is always the worst in comparison with the block and TM16 models. It is worth noting that for all types of models, the $\chi^2$ minimum value is reached for a reduction of 50% of Africa–Eurasia convergence, confirming the hypothesis that a significant part of the Africa–Eurasia convergence is absorbed through the Calabrian subduction, as proposed by Marotta & Sabadini (2008).

## Final remarks

A thermorheological analysis is performed to study the rheological structure of the lithosphere in the Mediterranean. Our results show that a strong lithosphere paves the Tyrrhenian, with a crust strongly coupled with mantle below the Provencal Basin and the Calabrian Arc surroundings, and the concurrence of hot lithosphere and thick crust in the Pannonian Area drives an average soft lithosphere. Furthermore, the southern portion of the Adria microplate can be rheologically differentiated from the northern portion, with the northern block stiffer than the southern one by about half an order of magnitude.

Once the predicted lithosphere stiffness is included within a tectonic model, the results confirm the crucial role played by the lateral rheological heterogeneities when deformation is analysed at the short wavelengths of a few hundred of kilometres.

In fact, strong rheological gradients concur with crustal and lithosphere thickness variations to drive a diffuse SW–NE extension within the regional context of active Africa–Eurasia convergence. In particular, tectonic model TM16_50, accounting for 50% of Africa–Eurasia convergence transmitted through the Calabrian subduction zone, predicts extension in Sicily, southern Calabria and part of the southern Tyrrhenian, as well as compression in the Algerian region, as shown by the World Stress Map 2008 compilation. A $\chi^2$ analysis confirms this hypothesis that a significant part of the Africa–Eurasia convergence is absorbed through the Calabrian subduction, as already proposed by Marotta & Sabadini (2008).

This work was supported by the Italian Space Agency project *SISMA*. The authors thank the editor and the reviewers I. Jiménez-Munt and U. Bayer for their constructive criticisms. All figures have been created by GMT plotting software (Wessel & Smith 2001).

## References

AFONSO, J. C. & RANALLI, G. 2004. Crust and mantle strengths in continental lithosphere; is the jelly sandwich model obsolete? *Tectonophysics*, **394**(3–4), 221–232.

ALTAMIMI, Z., COLLILIEUX, X., LEGRAND, J., GARAYT, B. & BOUCHER, C. 2007. ITRF2005: A new release of the International Terrestrial Reference Frame based on time series of station positions and Earth Orientation Parameters. *Journal of Geophysical Research*, **112**, B09401, doi: 10.1029/2007JB004949.

ARTEMIEVA, I. M. 2006. Global 1° × 1° thermal model Tc1 for the continental lithosphere: implications for lithosphere secular evolution. *Tectonophysics*, **416**, 245–277.

ARTEMIEVA, I. M. & MOONEY, W. D. 2001. Thermal thickness and evolution of Precambrian lithosphere: a

global study. *Journal of Geophysical Research*, **106**, B8, 16,387–16,414.

BASSIN, C., LASKE, G. & MANSTER, G. 2000. The current limit of resolution for surface wave tomography in North America. *Eos, Transactions of the American Geophysical Union*, **81**(48), Abstract S12A-03.

BLEWITT, G. & LAVALLÉE, D. 2002. Effect of annual signal on geodetic velocities. *Journal of Geophysical Research*, **107**(B7), 2145.

CANNIZZARO, L. 2008. *Analysis of Temporal Correlations in GPS Time Series: Comparison Between Different Methods at Different Space Scale*. PhD thesis, Polytechnic of Milan.

CHOPRA, P. N. & PETERSON, M. S. 1981. The experimental deformation of dunite. *Tectonophysics*, **78**, 453–473.

DACH, R., HUGENTOBLER, U., FRIDEZ, P. & MEINDL, A. (eds) 2007. *Bernese GPS Software Version 5.0*. Astronomical Institute, University of Bern.

DEVOTI, R., FERRARO, C. *ET AL*. 2002. Geodetic control on recent tectonic movements in the central Mediterranean area. *Tectonophysics*, **346**, 151–167.

DEMETS, C. & DIXON, T. H. 1999. New kinematic models for Pacific-North America motion from 3 Ma to present; Evidence for steady motion and biases in the NUVEL-1A model. *Geophysical Research Letters*, **26**, 1921–1924.

DEMETS, C., GORDON, R.G, ARGUS, D. F. & STEIN, S. 1994. Effects of recent revision to the geomagnetic reversal timescale on estimates of current plate motion. *Geophysical Research Letters*, **21**, 2191–2194.

DONG, D., FANG, P., BOCK, Y., CHENG, M. K. & MIYAZAKY, S. 2002. Anatomy of apparent seasonal variations from GPS-derived site position time series. *Journal of Geophysical Research*, **107**, (B4), 2075.

FERNANDES, R. M. S., AMBROSIUS, B. A. C., NOOMEN, R., BASTOS, L., WORTEL, M. J. R., SPAKMAN, W. & GOVERS, R. 2003. The relative motion between Africa and Eurasia as derived from ITRF2000 and GPS data. *Geophysical Research Letters*, **30**, 1828; doi: 10.1029/2003GL017089.

HEIDBACH, O., TINGAY, M., BARTH, A., REINECKER, J., KURFEß, D. & MÜLLER, B. 2008. *The release 2008 of the World Stress Map* (available online at www.world-stress-map.org).

HUGENOBLER, U., SHAER, S. *ET AL*. 2000. CODE IGS Analysis Center Technical Report. *In*: GOWEY, K., NEILAN, R. & MOORE, A. (eds) *IGS 2000 Technical Reports*. Jet Propulsion Laboratory Publication, **02-012**, 73.

JIMENEZ-MUNT, I., SABADINI, R., GARDI, A. & BIANCO, G. 2003. Active deformation in the Mediterranean from Gibraltar to Anatolia inferred from numerical modeling, geodetic and seismological data. *Journal of Geophysical Research*, **108**(B1), 2006; doi: 109/2001JB001544.

KREMER, C., HOLT, W. E. & HAINES, A. J. 2003. An integrated global model of present-day plate motions and plate boundary deformation. *Geophysical Journal International*, **154**, 8–34.

MAROTTA, A. M. & SABADINI, R. 2008. Africa–Eurasia kinematics control of long-wavelength tectonic deformation in the Central Mediterranean. *Geophysical Journal International*, **175**, 742–754.

MAROTTA, A. M., MITROVICA, J. X., SABADINI, R. & MILNE, G. 2004. Combined effects of tectonics and glacial isostatic adjustment on intraplate deformation in central and northern Europe: applications to geodetic baseline analyses. *Journal of Geophysical Research*, **109**, B01413, doi: 10.1029/2002JB002337.

MCCLUSKY, S., BALASSANIAN, S. *ET AL*. 2000. Global Positioning System constraints on plate kinematics and dynamics in the eastern Mediterranean and Caucasus. *Journal of Geophysical Research*, **105**, 5695–5719.

MCCLUSKY, S., REILINGER, R., MAHMOUD, S., BEN SARI, D. & TEALEB, A. 2003. GPS constrains on Africa (Nubia) and Arabia plate motions. *Geophysical Journal International*, **155**, 126–138.

NEGREDO, A. M., JIMÉNEZ-MUNT, I. & VILLASENOR, A. 2004. Evidence for eastward mantle flowbeneath the Caribbean plate from neotectonic modeling. *Geophysical Research Letters*, **31**, L06615; doi: 10.1029/2003GL019315.

NIKOLAIDIS, R. 2002. *Observation of Geodetic and Seismic Deformation with the Global Positioning System*. PhD thesis, University of California, San Diego, CA.

NOCQUET, J.-M. & CALAIS, E. 2003. Crustal velocity field of western Europe from permanent GPS array solutions, 1996–2001. *Geophysical Journal International*, **154**, 72–88.

NOCQUET, J. M., CALAIS, E., ALTAMINI, A., SILLARD, P. & BOUCHER, C. 2001. Intraplate deformation in western Europe deduced from an analysis of the International Terrestrial Reference Frame 1997 (ITRF97) velocity field. *Journal of Geophysical Research*, **106**(B6), 11,239–11,257.

OLDOW, J. S., FERRANTI, L. *ET AL*. 2002. Active fragmentation of Adria, the north African promontory, central Mediterranean orogen. *Geology*, **30**, 779–782.

POLLACK, H. N. & CHAPMAN, D. S. 1977. On the regional variation of heat flow, geotherms, and lithospheric thickness. *Tectonophysics*, **38**, 279–296.

POLLACK, H. N., HURTER, S. & JOHNSON, J. R. 1993. Heat flow from the Earth's interior: analysis of the global data set. *Reviews of Geophysics*, **31**(3), 267–280.

RANALLI, G. & MURPHY, D. C. 1987. Rheological stratification of the lithosphere. *Tectonophysics*, **132**, 281–295.

RAY, J., ALTAMIMI, Z., COLLILIEUX, X. & VAN DAM, T. 2008. Anomalous harmonics in the spectra of GPS position estimates. *GPS Solutions*, **12**, 55–64.

SELLA, F. G., DIXON, T. H. & MAO, A. 2002. REVEL: A model for Recent plate velocities from space geodesy. *Journal of Geophysical Research*, **107**(B4), 2081; doi: 10.1029/2000JB000033.

TESAURO, M., KABAN, M. K. & CLOETINGH, S.A.P.L. 2008. EuCRUST-07: a new reference model for the European crust. *Geophysical Research Letters*, **35**, L0S313; doi: 10.1029/2007JL032244.

WANG, J. & ZHENG-REN, Y. 2006. Dynamic modeling for crustal deformation in China: comparisons between the theoretical prediction and the recent GPS data. *Physics of the Earth and Planetary Interior*, **155**, 201–207.

WEERTMAN, J. & WEERTMAN, J. R. 1975. High temperature creep of rock, and mantle viscosity. *Annual Review of Earth and Planetary Sciences*, **3**, 293–315.

WESSEL, P. & SMITH, W. M. F. 2001. New improved version of generic mapping tools released. *Eos, Transactions of the American Geophysical Union*, **79**, 579.